Inorganic Chemistry

pubs.acs.org/IC

Article

Chromate Incarceration by Nanojars and Its Removal from Water by Liquid−Liquid Extraction

Wisam A. Al Isawi, Christian K. Hartman, Pooja Singh, Matthias Zeller, and Gellert Mezei*

Cite This: *Inorg. Chem.* 2023, 62, 5716−5728

Read Online

ACCESS | Metrics & More | Article Recommendations | Supporting Information

ABSTRACT: The unprecedented liquid−liquid extraction of the dinegative chromate ion (CrO_4^{2-}) from neutral aqueous solutions into aliphatic hydrocarbon solvents using nanojars as extraction agents is demonstrated. Transferring chromate from water into an organic solvent is extremely challenging due to its large hydration energy (ΔG_h° = −950 kJ/mol) and strong oxidizing ability. Owing to their highly hydrophilic anion binding pockets lined by a multitude of hydrogen bond donor OH groups, neutral nanojars of the formula $[cis\text{-}Cu^{II}(\mu\text{-OH})(\mu\text{-4-Rpz})]_n$ (n = 27−33; pz = pyrazolate anion; R = H or *n*-octyl) strongly bind the CrO_4^{2-} ion and efficiently transfer it from water into *n*-heptane or C_{11} − C_{13} isoalkanes (when R = *n*-octyl). The extracted chromate can easily be recovered from the organic layer by stripping with an aqueous acid solution. Electrospray ionization mass spectrometric, UV−vis and paramagnetic ^{1}H NMR spectroscopic, X-ray crystallographic, and thermal stability studies in solution and chemical stability studies toward NH_3, methanol, and Ba^{2+} ions are employed to explore the binding of the CrO_4^{2-} ion by nanojars. Titration of carbonate nanojars $[CO_3 \subset \{Cu(OH)(pz)\}_n]^{2-}$ with H_2CrO_4 leads to anion exchange and the formation of chromate nanojars $[CrO_4 \subset \{Cu(OH)(pz)\}_n]^{2-}$. Details of chromate binding by H-bonding based on single-crystal structures of $(Bu_4N)_2[CrO_4 \subset \{Cu(OH)(pz)\}_{28}]$, four pseudopolymorphs of $(Bu_4N)_2[CrO_4 \subset \{Cu(OH)(pz)\}_{31}]$, and also the methoxy-substituted derivative $(Bu_4N)_2[CrO_4 \subset \{Cu_{31}(OH)_{30}(OCH_3)(pz)_{31}\}]$ are presented.

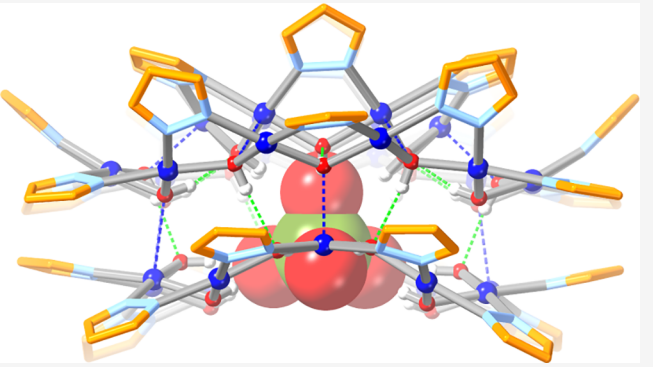

INTRODUCTION

Inorganic oxoanions are common contaminants in water supplies around the world. Some of these oxoanions originate from natural sources while others are byproducts of industrial processes. Cr(VI) oxoanions, including chromate (CrO_4^{2-}), hydrogen chromate ($HCrO_4^-$), and dichromate ($Cr_2O_7^{2-}$), pose a serious threat to living organisms as Cr(VI) is highly toxic, mutagenic, teratogenic, and carcinogenic.[1,2] Although chromium is quite abundant in Earth's crust (21st most abundant element with an average concentration of 102 ppm),[3] most chromium minerals contain the non-toxic Cr(III) ion. Chromate-containing minerals, of which at least 22 different examples are known, are rare.[4] Nevertheless, high levels of chromate can occur in aquifers under oxidizing conditions, where Cr(III) is naturally oxidized to Cr(VI).[5−9] Chromium pollution is most often associated with industrial applications, such as chrome plating and chromate conversion coating, corrosion inhibition, alloy production, leather tanning, wood preservation, refractory bricks, pigments, textile dyes and mordants, mineral ore, and petroleum refining.[10−15]

According to the current regulations of the U. S. Environmental Protection Agency, chromium concentration in drinking water should not exceed 100 ppb.[16] Chromate is currently removed from drinking water either by reduction with $FeSO_4$ followed by precipitation, coagulation, and filtration of the resulting insoluble Cr(III) hydroxide,[17] or by adsorption onto ion exchange resins or polymeric adsorbents.[18−20] These methods can efficiently remove chromate from solutions, but they suffer from drawbacks. If filtration leaves behind any Cr(III), this will be re-oxidized to Cr(VI) during subsequent disinfection by chlorination. Large-scale use of ion exchange resins is costly, and filtration and adsorption onto polymeric adsorbents generate contaminated side-products. Other solid-phase methods of chromate removal have also been explored, including binding onto magnetic nanoparticle surfaces,[21,22] metal-organic[23,24] or ionic covalent organic frameworks,[25,26] and separation by crystallization as a bis(iminoguanidinium) salt.[27]

An alternative way of removing chromate from water is by liquid−liquid extraction into an immiscible organic layer using

Received: January 24, 2023
Published: March 24, 2023

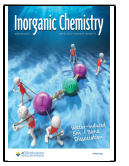

extracting agents such as quaternary ammonium salts,[28−32] trioctylphosphine oxide,[33] tributyl phosphate,[34] and calixarenes.[35−37] This method offers recyclability and easier recovery of the extracted chromate. However, it is difficult to transfer CrO_4^{2-} (which is the dominant form of chromate at neutral and alkaline pH values)[38] from water into organic solvents due to its large hydration energy (ΔG_h° = −950 kJ/mol).[39] Therefore, extractions of chromate have been carried out under highly acidic conditions, where CrO_4^{2-} is converted into more charge-diffuse species with much smaller hydration energies, such as $HCrO_4^-$, $Cr_2O_7^{2-}$, and $ClCrO_3^-$ (the latter in the presence of chloride ions). To extract CrO_4^{2-} from water under neutral or alkaline conditions, an extracting agent that is capable of overcoming the large hydration energy of CrO_4^{2-} is needed. Only a few supramolecular receptors are known to encapsulate CrO_4^{2-}, namely, azacryptands,[40,41] metal−organic cages based on bis-urea ligands,[42] dimeric capsules based on tripodal tris-urea receptors,[43,44] an azacalix[2]-dipyrrolylmethane macrocycle,[45] and Ag(I) clusters.[46,47] Only one of these receptors has been employed for the liquid−liquid extraction of CrO_4^{2-}, using a CH_2Cl_2/H_2O solvent system. Based on the experimental details provided, the residual chromate concentration in the aqueous phase after extraction is ∼380 ppm.[44] Of the CrO_4^{2-} binding host−guest complexes mentioned above, a binding constant has only been reported for a tripodal tris-urea receptor ($K_a \sim 10^4$ in DMSO-d_6/D_2O 9:1, v/v).[44] For comparison, the chromate binding constant of the sulfate-binding protein isolated from *Salmonella typhimurium* is $K_a = 3 \times 10^6$ in H_2O.[48] Another challenge in chromate binding is posed by the fact that chromate is a strong oxidizing agent that degrades many organic compounds. Protonated azacryptands, for example, are not stable in the presence of chromate.[40]

Herein, we describe a chromate extraction agent capable of lowering the CrO_4^{2-} ion concentration in water to below 100 ppb by liquid−liquid extraction into aliphatic hydrocarbon solvents. The extraction agent comprises a class of neutral supramolecular coordination complexes of the formula $[CrO_4 \subset \{cis\text{-}Cu^{II}(\mu\text{-}OH)(\mu\text{-}4\text{-}Rpz)\}_n]^{2-}$ (Cu_nCrO_4; n = 27−33; pz = pyrazolate, $C_3H_3N_2^-$; R = H or *n*-octyl), termed nanojars (Scheme 1).[49] Nanojars consist of three stacked $[cis\text{-}Cu^{II}(\mu\text{-}OH)(\mu\text{-}pz)]_x$ metallamacrocycles (x = 6−10 for the two side-rings, and 12−14 for the central ring) held together by multiple H-bonds and axial Cu···O interactions.[50,51] Electrospray ionization mass spectrometric (ESI-MS), UV−vis and variable-temperature, paramagnetic nuclear magnetic resonance (^{1}H NMR) spectroscopic, X-ray crystallographic, anion binding, and reactivity studies have been performed to characterize chromate-binding nanojars.

RESULTS AND DISCUSSION

Synthesis and Mass Spectrometric Studies. Mixtures of CrO_4-incarcerating nanojars of the formula $(Bu_4N)_2[CrO_4 \subset \{cis\text{-}Cu^{II}(\mu\text{-}OH)(\mu\text{-}pz)\}_n]$ (Cu_nCrO_4; n = 27−33) were obtained from the reaction of $Cu(NO_3)_2$ with pyrazole, NaOH, Bu_4NOH, and Na_2CrO_4 (1:1:2:0.07:1 molar ratio) in tetrahydrofuran (THF) at ambient temperature. ESI-MS(−) analysis indicates that the mixture consists mainly of nanojars with n = 28 (m/z 2125), n = 30 (m/z 2272), n = 31 (m/z 2346), and n = 32 (m/z 2420), with small amounts of nanojars with n = 27 (m/z 2051), n = 29 (m/z 2199), and n = 33 (m/z 2494) (Figure 1). Similar results were obtained using copper(II) chromate instead of $Cu(NO_3)_2/Na_2CrO_4$. Based on its lower solubility in toluene, the smaller $Cu_{28}CrO_4$ nanojar can be separated from the larger nanojars by selective crystallization. Thus, when a clear solution of Cu_nCrO_4 (n = 27−33) in toluene is left standing in a closed vessel for 48 h, a precipitate forms, which is identified by ESI-MS(−) as mostly $Cu_{28}CrO_4$, with small amounts of $Cu_{31}CrO_4$ and $Cu_{32}CrO_4$ (Figure 2b). On the contrary, the filtrate contains the larger nanojars, with only a small amount of $Cu_{28}CrO_4$ (Figure 2c).

In the case of the sulfate and tetrafluoroberyllate nanojars, pure $Cu_{31}SO_4$ and $Cu_{31}BeF_4$ could be obtained by adding Pb^{2+} ions to the nanojar-forming reaction mixture, which form $PbSO_4$ or $PbBeF_4$.[52,53] The poor solubility ($PbSO_4$: 44 mg/L H_2O at 25 °C; $K_{sp} = 2.53 \times 10^{-8}$)[54] of these lead salts assures that there is only a small amount of Pb^{2+}(aq) ions present in the reaction mixture, which nevertheless provides enough acidity (pK_a = 7.6)[55] to break down the more vulnerable, smaller nanojars and lead to the formation of the more stable Cu_{31} nanojars. A more soluble Pb^{2+} salt provides too much acidity and results in complete breakdown of the nanojars.[56] In

Scheme 1. Schematic Representation of the Cu_{31} Nanojar, $[CrO_4 \subset \{Cu(OH)(pz)\}_{8+14+9}]^{2-}$[a]

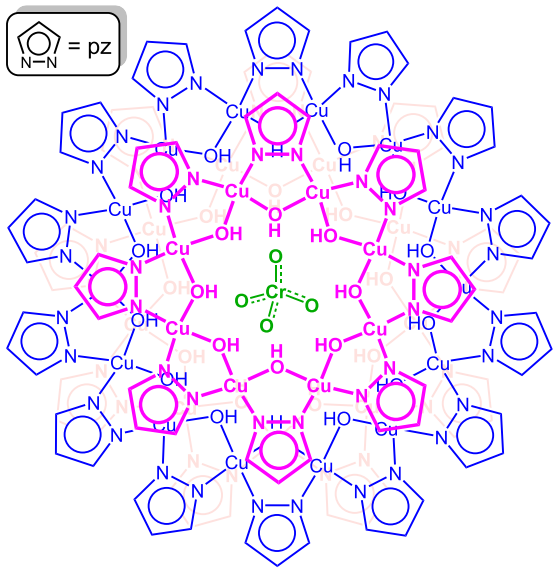

[a]Color code: magenta − Cu_8-ring; blue − Cu_{14}-ring; light red − Cu_9-ring.

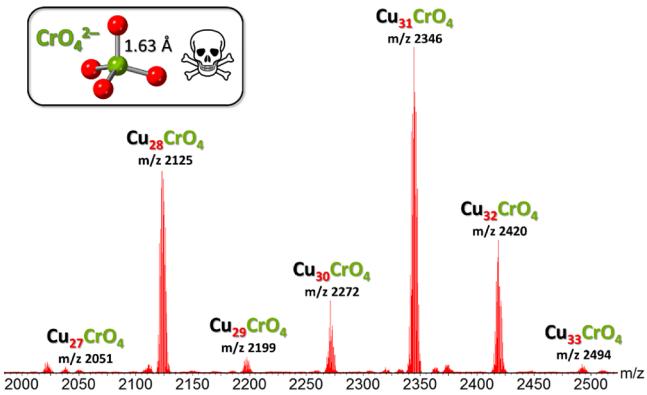

Figure 1. ESI-MS(−) spectrum of the as-synthesized chromate-incarcerating nanojar mixture $[CrO_4 \subset \{Cu(OH)(pz)\}_n]^{2-}$ (Cu_nCrO_4; n = 27−33) in CH_3CN. Detailed isotopic distributions are shown in Figure S1).

https://doi.org/10.1021/acs.inorgchem.3c00262
Inorg. Chem. 2023, 62, 5716−5728

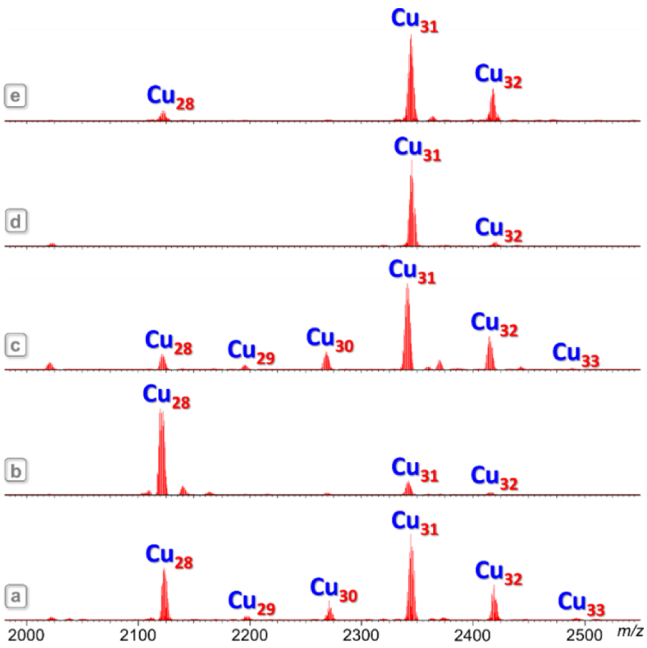

Figure 2. ESI-MS(−) spectra in CH_3CN of (a) the as-synthesized Cu_nCrO_4 (n = 27−33), (b) the fraction of Cu_nCrO_4 crystallized out of a toluene solution, (c) the fraction of Cu_nCrO_4 soluble in toluene, (d) the product obtained by NH_3(g) treatment of the Cu_nCrO_4 mixture in THF solution, and (e) the Cu_nCrO_4 mixture obtained by reacting Cu_nCO_3 (n = 27−31) with 2 equiv of H_2CrO_4.

contrast, $PbCrO_4$ has an extremely low solubility in water (0.17 mg/L H_2O at 20 °C; K_{sp} = 2.8 × 10^{-13})[57] and, as opposed to the more soluble $PbSO_4$ or $PbBeF_4$ salts, has no effect on the Cu_nCrO_4 mixture.

The reaction of the Cu_nCrO_4 mixture with NH_3, however, does proceed similarly to Cu_nSO_4 and Cu_nBeF_4. Thus, saturating a solution of Cu_nCrO_4 (n = 27−33) in THF with gaseous NH_3 leads to the conversion of all smaller nanojars to $Cu_{31}CrO_4$. In the ESI-MS(−) spectrum of the resulting product, a small amount of $Cu_{32}CrO_4$ is also noticeable (Figure 2D). It becomes apparent that the larger Cu_{32} nanojar, although it is not as preferred as $Cu_{31}CrO_4$, is more prevalent with the larger CrO_4^{2-} ion (Cr−O: 1.63 Å) than with the smaller SO_4^{2-} (S−O: 1.48 Å) or BeF_4^{2-} (Be−F: 1.55 Å) ions.

Conversion of Cu_nCO_3 to Cu_nCrO_4 Nanojars by Anion Exchange. On treatment with increasing equivalents of H_2CrO_4 (aqueous solution of CrO_3), carbonate nanojars $[CO_3 \subset \{Cu(OH)(pz)\}_n]^{2-}$ (Cu_nCO_3; n = 27, 29−31) gradually transform into chromate nanojars $[CrO_4 \subset \{Cu(OH)(pz)\}_n]^{2-}$ (Cu_nCrO_4; n = 31, 32) in a CH_3CN solution (Figure 3). Monitoring by ESI-MS(−) shows that at 1 equiv of H_2CrO_4, the $Cu_{30}CO_3$ and $Cu_{31}CO_3$ nanojars are absent, whereas the relative amounts of $Cu_{27}CO_3$ and $Cu_{29}CO_3$ nanojars remain the same and new peaks corresponding to $Cu_{31}CrO_4$ and $Cu_{32}CrO_4$ nanojars appear. This indicates that the larger Cu_nCO_3 (n = 30, 31) nanojars are the most sensitive to acidity, and in contrast, only the larger Cu_nCrO_4 (n = 31, 32) nanojars resist the acidic conditions. The absence of byproducts (lower nuclearity or insoluble species) also indicates that the smaller carbonate nanojars are cleanly converted into larger chromate nanojars either by anion exchange ($Cu_{8+14+9}CO_3$ into $Cu_{8+14+9}CrO_4$) or by nanojar rearrangement ($Cu_{8+14+8}CO_3$ and/or $Cu_{7+14+9}CO_3$ into $Cu_{8+14+10}CrO_4$ and/or $Cu_{9+14+9}CrO_4$). At 1.5 equiv of H_2CrO_4, the $Cu_{29}CO_3$ nanojars are also absent. Above 2 equiv of H_2CrO_4, only $Cu_{31}CrO_4$ and $Cu_{32}CrO_4$ nanojars are observed. At 2.5 equiv of H_2CrO_4, a new peak corresponding to $[CrO_4 \subset \{Cu_{31}(OH)_{31}(pz)_{30}(HCrO_4)\}(Bu_4N)(HCrO_4)]^{2-}$ (m/z 2550.87) also appears and becomes increasingly larger at higher equiv. of H_2CrO_4 (Figure S2). Apparently, at larger H_2CrO_4 concentrations, one pyrazolate group of the $Cu_{31}CrO_4$ nanojar is substituted by $HCrO_4^-$ and forms an adduct with $Bu_4N^+HCrO_4^-$. Above 2 equiv of H_2CrO_4, low-nuclearity peaks are also observed in the ESI-MS(−) spectrum, accompanied by partial precipitation (Figure S2). The clean conversion of Cu_nCO_3 to Cu_nCrO_4 by adding 2 equiv of H_2CrO_4 inspired a new method of synthesis of chromate nanojars (Figure 2e).

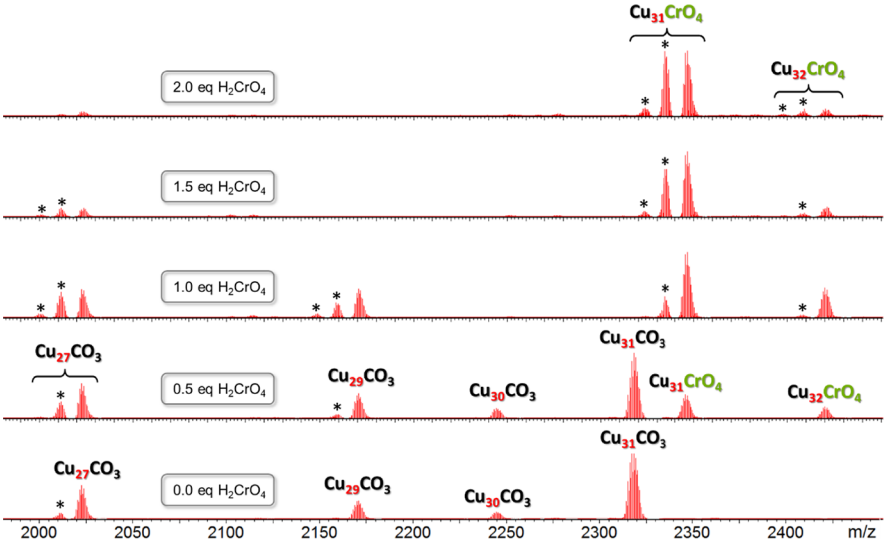

Figure 3. ESI-MS(−) spectra in CH_3CN of Cu_nCO_3 (n = 27, 29−31) nanojars with varying amounts of added H_2CrO_4. Beside the parent peaks, formate-substituted analogues (in which one or more pz^- moieties are substituted by $HCOO^-$, denoted by an asterisk) can also be observed at 11 m/z units less than the parent peak.

https://doi.org/10.1021/acs.inorgchem.3c00262
Inorg. Chem. 2023, 62, 5716−5728

The spectra shown in Figure 3 also indicate the presence of formate-substituted nanojars. As described earlier, nanojars are extremely sensitive to even traces of formic acid in the mass spectrometer (formic acid is commonly used as an additive to improve peak shapes and to promote ionization by producing $[M + H]^+$ ions).[58] Therefore, substituted nanojar species such as $[CrO_4^{2-} \subset \{Cu_{31}(OH)_{31}(pz)_{31-y}(HCOO)_y\}]$ (y = 1, m/z 2335; y = 2, m/z 2324) are sometimes found in the mass spectra. Formic acid can also result from the degradation of formaldehyde-based resins, which are used in vial caps.

Reaction of Nanojars with MeOH. The initially blue solutions of Cu_nCO_3 and Cu_nSO_4 in methanol gradually lose color and deposit an intractable, brown-gray solid at ambient temperature. In contrast, the appearance of a dilute solution of chromate-nanojars (Cu_nCrO_4; n = 27−33) in methanol remains unchanged on standing and ESI-MS(−) indicates the presence of methylated species $[CrO_4 \subset \{Cu_n(OH)_{n-1}(OMe)(pz)\}_n]^{2-}$ ($Cu_nCrO_4(OMe)$; n = 28, m/z 2132; n = 31, m/z 2353), along with low-nuclearity species in the m/z 600−1500 window (Figure S3b). Chromate nanojars with n = 29, 30, and 33 break down in methanol solution. When a more concentrated solution of Cu_nCrO_4 is prepared in methanol, a blue solid crystallizes out, which is composed mostly of $Cu_{31}CrO_4$ with small amounts of $Cu_{28}CrO_4$ and $Cu_{32}CrO_4$ (Figure S3c), whereas the mother liquor contains $Cu_{31}CrO_4(OMe)$ (and trace amounts of $Cu_{28}CrO_4(OMe)$), along with low-nuclearity species at m/z 1399 and 1435 (Figure S3d). Based on their isotopic pattern, these hitherto unidentified species appear to contain approx. six Cu atoms and no chromate, as the same species are also observed in the spectra of fresh methanolic solutions of Cu_nCO_3 and Cu_nSO_4. According to the ESI-MS studies, Cu_nCrO_4 species are monomethylated in solution in the presence of methanol to $Cu_nCrO_4(OMe)$, but they revert back to Cu_nCrO_4 when the solvent is evaporated or when the crystallized solid is removed from the solution and allowed to dry in the ambient air. Nevertheless, we were able to isolate single crystals of $Cu_{31}CrO_4(OMe)$ grown from a nitrobenzene/bromobenzene (1:1) solution of Cu_nCrO_4 (n = 27−33) by methanol vapor diffusion or from a nitrobenzene/methanol (1:1) solution, by quickly transferring them under a cryostream cooler at 150 K. The X-ray crystal structure of the latter is described in the crystallography section below.

Under reflux conditions in a methanol solution, Cu_nCrO_4 (n = 27−33) leads to the formation of a small amount of a brown precipitate similar to the ones obtained from Cu_nCO_3 and Cu_nSO_4 in methanol at room temperature. ESI-MS(−) of the blue filtrate shows exclusively $Cu_{31}CrO_4(OMe)$ (Figure 4b), without any low-nuclearity species in the m/z 600−1500 window. After solvent removal, ESI-MS(−) of the solid residue indicates conversion to $Cu_{31}CrO_4$ (Figure 4c). The identity of the solid was also confirmed by ^{1}H NMR spectroscopy (see the NMR section below).

Structural Analysis by X-ray Crystallography. Single-crystal X-ray diffraction analyses of $(Bu_4N)_2[CrO_4 \subset \{cis\text{-}Cu^{II}(\mu\text{-}OH)(\mu\text{-}pz)\}_{6+12+10}]$ ($Cu_{28}CrO_4$, **1**), four pseudopolymorphs of $(Bu_4N)_2[CrO_4 \subset \{cis\text{-}Cu^{II}(\mu\text{-}OH)(\mu\text{-}pz)\}_{8+14+9}]$ ($Cu_{31}CrO_4$, **2a** − chlorobenzene/pentane; **2b** − chlorobenzene/hexanes; **2c** − toluene/pentane; **2d** − nitrobenzene/bromobenzene), and also the methoxy-substituted derivative $(Bu_4N)_2[CrO_4 \subset \{cis\text{-}Cu^{II}{}_{31}(\mu\text{-}OH)_{30}(\mu\text{-}OCH_3)(\mu\text{-}pz)_{31}\}]$ ($Cu_{31}CrO_4(OMe)$, **3**) offer intricate details about the supramolecular binding of CrO_4^{2-} inside the hydrophilic nanojar cavity lined with H-bond donors (Figure 5, Tables S1−S19).

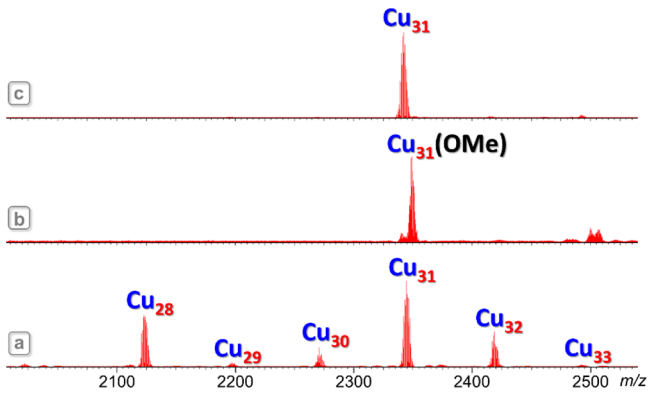

Figure 4. ESI-MS(−) spectra in CH_3CN of (a) the as-synthesized Cu_nCrO_4 (n = 27−33), (b) an aliquot of the methanol solution of Cu_nCrO_4 refluxed for 10 h, and (c) the solid product obtained after evaporating the methanol solvent from the refluxed solution.

In the triclinic ($P\bar{1}$) lattice of **1**, the nanojar unit is located on a general position and displays pseudo-symmetry relative to two orthogonal mirror planes (Figure 6). True symmetry is not attained due to the position of the incarcerated anion relative to the nanojar framework. Although the tetrahedral structure of an individual CrO_4^{2-} ion does allow symmetry relative to two orthogonal mirror planes, optimal hydrogen bonding within the cavity of the $Cu_{6+12+10}$ nanojar favors a position for the CrO_4^{2-} ion that is only symmetrical to one mirror plane. Thus, one O atom of CrO_4^{2-} is pointed toward and forms six H-bonds with the Cu_6 ring, whereas the other three O atoms are oriented toward the Cu_{10} ring and each one forms three H bonds (with D···A distances <3.2 Å). It should be noted that the CrO_4^{2-} ion is found disordered within the nanojar cavity in a 62/19/19 ratio, with the major part (62%) being the favored position described above. In one minor position (19%), the CrO_4^{2-} ion binds similarly but is rotated by ∼60° roughly around the pseudo-C_3 axis running through the Cr atom and the O atom oriented toward the Cu_6 ring. In this orientation, one O atom still forms six H-bonds with the Cu_6 ring, but of the other three O atoms, only one forms three H bonds with the Cu_{10} ring and the other two form only two H-bonds. In the second minor orientation (19%), the CrO_4^{2-} ion is positioned almost symmetrically relative to the two orthogonal mirror planes (Figure 6). In this orientation, two O atoms of the CrO_4^{2-} ion form two H-bonds each with the Cu_6 ring, and the other two O atoms form three H-bonds each with the Cu_{10} ring. The Cu_{12} ring is too large for its OH groups to form H-bonds with the CrO_4^{2-} ion. Instead, its OH groups form alternating H-bonds with the adjacent Cu_6 and Cu_{10} rings.

Although the molecular structure of the $Cu_{28}CrO_4$ nanojar is very similar to the sulfate[52] and tetrafluoroberyllate[53] analogues, the crystal structure of **1** is not isomorphous with the ones of the previously described $Cu_{28}SO_4$ and $Cu_{28}BeF_4$ (the latter two are isomorphous, also triclinic $P\bar{1}$, but with different unit cell parameters). The difference originates from the different orientation of the Bu_4N^+ counterion adjacent to the Cu_{10} ring. As shown in Figure S11, the Bu_4N^+ moiety is centered on top of the Cu_{10} ring in $Cu_{28}SO_4$ and $Cu_{28}BeF_4$, whereas in $Cu_{28}CrO_4$, it is offset, altering the overall packing pattern of the nanojar units (Figure S12).

https://doi.org/10.1021/acs.inorgchem.3c00262
Inorg. Chem. 2023, 62, 5716−5728

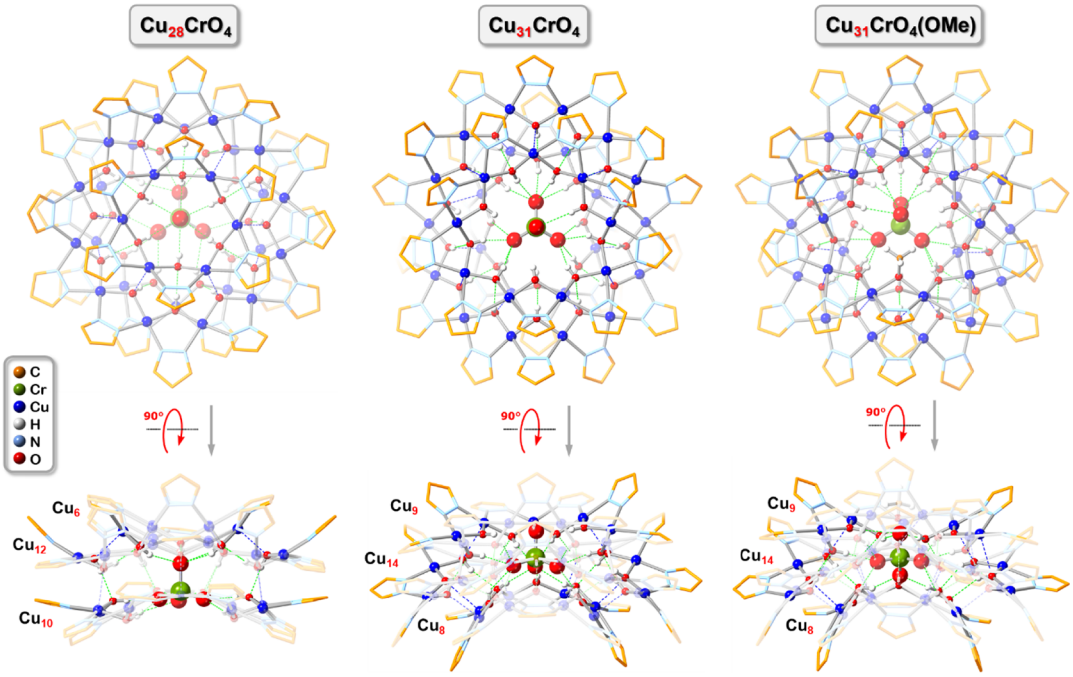

Figure 5. Ball-and-stick representation of the crystal structures of **1**−**3** (top- and side-views). Green and blue dotted lines indicate hydrogen bonds and axial Cu···O interactions, respectively. Counterions, lattice solvent molecules and C−H bond H-atoms are omitted for clarity, and only the major component is shown for disordered moieties.

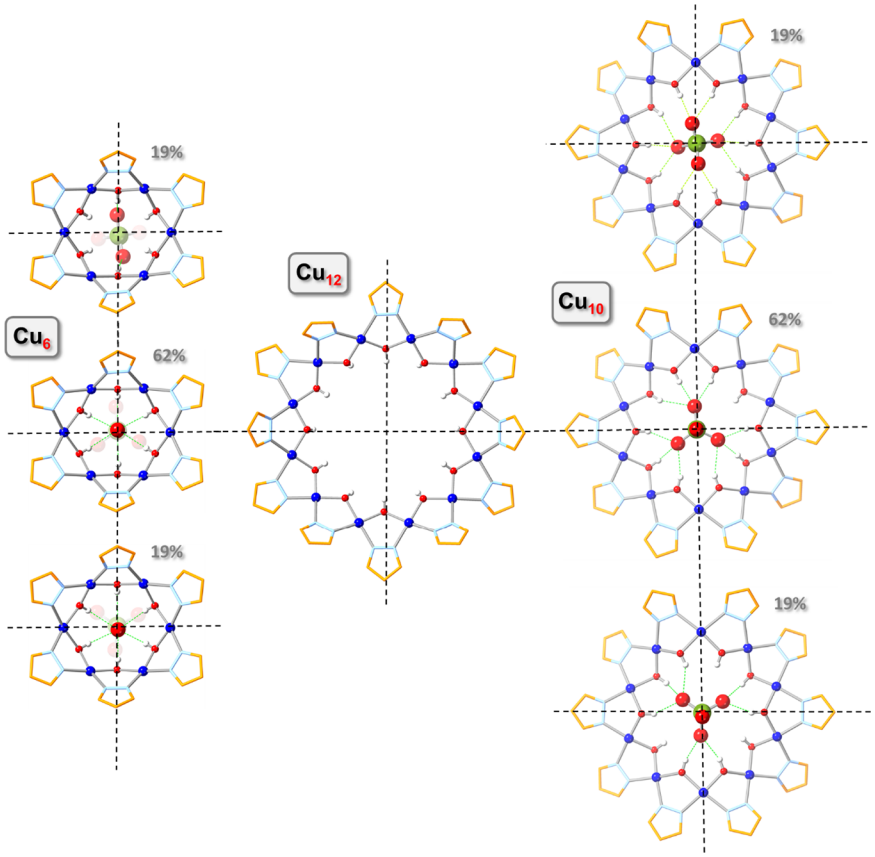

Figure 6. Illustration of the pseudo-mirror-planes bisecting the Cu_6, Cu_{12}, and Cu_{10} rings in **1**, as well as the hydrogen bonding pattern (green dashed lines) between CrO_4^{2-} and the Cu_6 and Cu_{10} rings.

The $Cu_{31}CrO_4$ nanojar is also located on a general position in **2a**−**d** (triclinic $P\bar{1}$), but in contrast to $Cu_{28}CrO_4$ (**1**), only its Cu_8 ring displays pseudo-symmetry relative to two orthogonal mirror planes, whereas the Cu_9 and Cu_{14} rings are pseudo-symmetrical relative to only one mirror plane (Figure S13). The CrO_4^{2-} ion is found mostly in one position

https://doi.org/10.1021/acs.inorgchem.3c00262
Inorg. Chem. 2023, 62, 5716−5728

(95%) in **2a**, with a minor disordered component (5%). In the major orientation, one O atom of the CrO_4^{2-} ion is poking out through the Cu_9 ring and forms one H-bond with it, whereas its other three O atoms form H bonds with both the Cu_9 and Cu_8 rings (2 + 2 H bonds each except one O atom that forms 2 + 3 H bonds with the Cu_9 and Cu_8 rings, respectively). In the minor orientation, the CrO_4^{2-} ion is roughly inverted so that one O atom is pointing toward the Cu_8 ring and forms three H-bonds with it, two O atoms are pointing toward the Cu_9 ring and form three H-bonds each with it, and the fourth O atom is in between the Cu_9 and Cu_8 rings and forms two H-bonds with each. Again, the large Cu_{14} ring does not bind to the CrO_4^{2-} ion but it forms alternating H-bonds with the adjacent Cu_8 and Cu_9 rings. In **2b** and **2c**, which are isomorphous with **2a**, the CrO_4^{2-} ion is not disordered and it is found in the same orientation and H-bonding environment as the major component in **2a**. **2d** is not isomorphous with **2a**–**c** and two crystallographically independent nanojar moieties are found in its asymmetric unit. In unit 1, the CrO_4^{2-} ion is disordered in a 0.89/0.11 ratio (similarly to **2a**), whereas in unit 2, it is not disordered (similarly to **2b** and **2c**). Although the position of the two Bu_4N^+ counterions relative to the nanojar units is similar to the ones in **2a**–**c** (Figure S14), the packing diagram of **2d** is quite different (Figure S15).

The substitution of one OH group of the Cu_9 ring in $Cu_{31}CrO_4$ by an OMe group leaves the nanojar framework, which is located in a general position in $Cu_{31}CrO_4(OMe)$ (**3**), practically unaffected (Figure 5). The presence of the OMe group, however, changes the position of the CrO_4^{2-} ion within the nanojar cavity and its H-bonding pattern, as well as the surroundings of the nanojar. As shown in Figure 7, the OMe

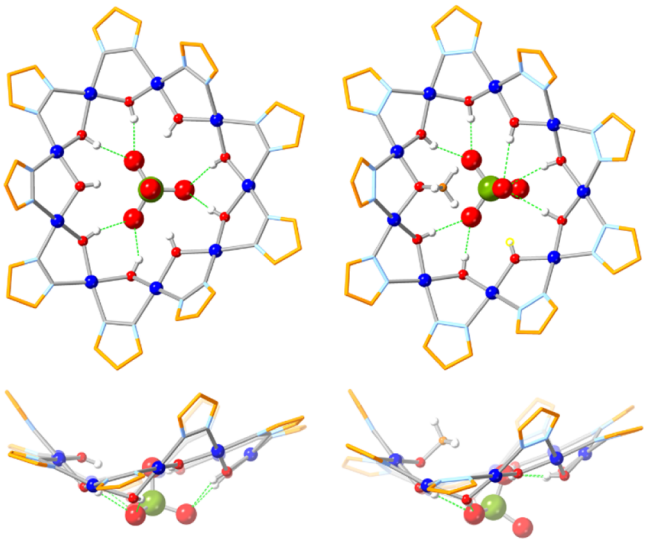

Figure 7. Comparison (top and side views) between the $Cu_9(OH)_9(pz)_9$ and $Cu_9(OMe)(OH)_8(pz)_9$ metallamacrocycles observed in **2** (left) and **3** (right), respectively, illustrating the change in the position of the CrO_4^{2-} ion and the corresponding H-bonds.

group pushes away the O atom of the CrO_4^{2-} ion, which pokes through the Cu_9 ring so that the corresponding O···O distance increases from 3.170(4)–3.333(6) Å in **2a**–**d** to 3.838(4) Å in **3**. Consequently, the Bu_4N^+ counterion located next to the Cu_9 ring shifts position (Figure 8) and alters the packing of nanojars in the crystal lattice (which remains triclinic $P\bar{1}$, but with different unit cell parameters than in **2a**–**d**) (Figure S16).

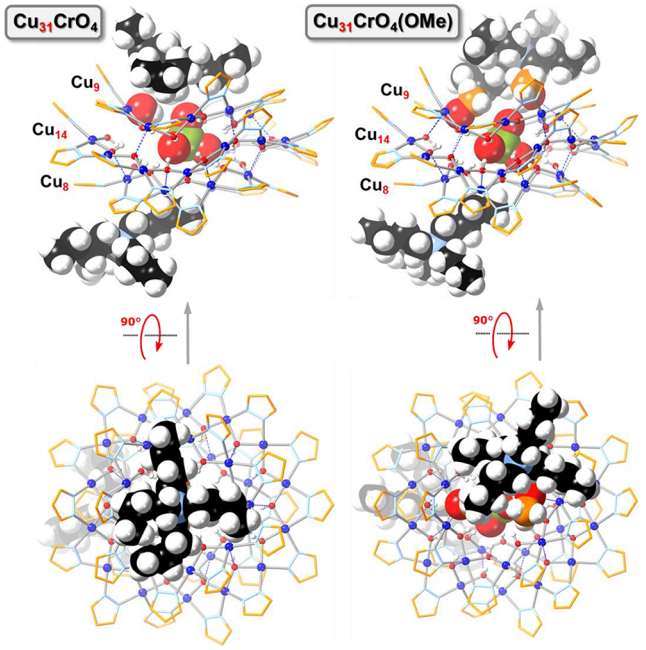

Figure 8. Comparison of the X-ray crystal structures of $Cu_{31}CrO_4$ (**2a**–**c**) and $Cu_{31}CrO_4(OMe)$ (**3**). Pyrazole H atoms are omitted for clarity and only the major component is shown for disordered moieties.

Because the OMe group is located on the pseudo-mirror plane bisecting the nanojar, the symmetry of the $Cu_{31}CrO_4(OMe)$ nanojar remains the same as that of $Cu_{31}CrO_4$ (Figure S17). Due to the tilting of the CrO_4^{2-} ion within the nanojar cavity in **3**, the H-bonding pattern changes slightly in **3** compared to **2**. Thus, the O atom that in **2** formed 2 + 3 H-bonds with the Cu_9 and Cu_8 rings, respectively, loses the two H-bonds with the Cu_9 ring in **3**. In addition, a MeOH molecule is now occupying the space opened up by the shifting of the Bu_4N^+ moiety and forms an H-bond with the O atom of the CrO_4^{2-} ion, which was pushed away by the coordinated OMe group.

In terms of structural parameters within the Cu_x-rings of **1**–**3**, only minor differences are observed with consistent average Cu–O bond lengths of 1.924(2)–1.930(3) Å, average Cu – N bond lengths of 1.974(3)–1.977(3) Å, average *trans* and *cis* N–Cu–O angles of 171.4(1)–172.2(2)° and 85.5(2)–85.8(1)°, respectively, and average Cu···Cu distances of 3.288(1)–3.303(1) Å (Tables S3, S4, and S6–S12). The non-covalent interactions between individual Cu_n-rings are comparable, with average axial Cu···O distances of 2.478(3)–2.574(3) Å, and average H-bonded O···O distances of 2.789(4)–2.872(4) Å. The H-bonding parameters between Cu_n-rings and the incarcerated CrO_4^{2-} anion are also comparable, with average O···O distances ranging from 2.917(3) Å to 2.935(5) Å (Tables S13–S19). Moreover, the dihedral angles and the component fold- and twist-angles between the mean planes of the pyrazolate moiety and the three atoms of the Cu–O–Cu unit (as defined earlier)[59] were analyzed (Table S5). Thus, the average fold angles in the larger, flatter central rings (Cu_{12} or Cu_{14}) are 40.7(2)–43.7(2)° in **1**–**3**, whereas in the two smaller, more puckered side-rings the values are 48.6(2)–55.8(2)° (Cu_9 or Cu_{10}) and 45.3(2)–50.8(2)° (Cu_6 or Cu_8). The corresponding average twist angles are 5.0(2)–5.9(2)° in the central rings (Cu_{12} or Cu_{14}) and 3.1(2)–5.4(2)° (Cu_9 or Cu_{10}) and 2.1(2)–4.5(2)°

https://doi.org/10.1021/acs.inorgchem.3c00262
Inorg. Chem. 2023, 62, 5716–5728

(Cu_6 or Cu_8) in the two side-rings. Similar to the Cu_nSO_4 and Cu_nBeF_4 analogues, only small variations of <8° and < 3° are observed for the fold and twist angle averages, respectively, despite the pronounced variations of 79° and 16° between the individual fold (0.7(3)−79.6(2)°) and twist angles (0.0(2)−15.8(2)°).

^{1}H NMR Spectroscopy. Consistent with the ESI-MS characterization detailed above, the ^{1}H NMR spectrum of the Cu_nCrO_4 (n = 27−33) nanojar mixture in DMSO-d_6 displays two major sets of peaks corresponding to $Cu_{6+12+10}CrO_4$ and $Cu_{8+14+9}CrO_4$ as well as minor peaks corresponding to the other nanojar sizes (Figure 9, Figure S18, Table S20). The

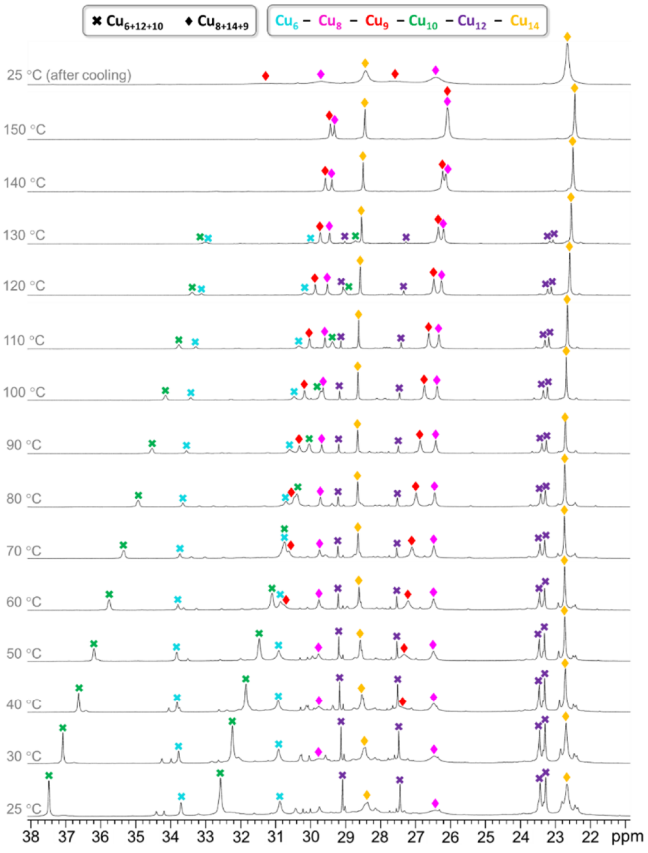

Figure 9. Variable-temperature ^{1}H NMR spectra of the Cu_nCrO_4 (n = 27−33) nanojar mixture in DMSO-d_6, showing pyrazolate proton signals in the 22−38 ppm window. The given temperatures are the target temperatures of the probe.

spectrum of Cu_nCrO_4 is similar to the ones of Cu_nSO_4 and Cu_nBeF_4,[52,53] in terms of the drastic downfield shift of the pyrazolate proton peaks (between 22 and 38 ppm at 25 °C) and the even more drastic upfield shift of the OH proton peaks (between −26 and −55 ppm at 25 °C), as well as the broadening of the peaks and loss of the J coupling between nuclei, all due to the paramagnetism of the Cu^{2+} centers. The most affected peaks are those of the Cu_{10}-ring of the $Cu_{28}CrO_4$ nanojar: the one corresponding to the 4-position of the pz moieties appears at 37.48 ppm, whereas the one corresponding to the OH protons appears at −54.03 ppm. The most striking difference between the spectra of Cu_nCrO_4 and the corresponding Cu_nSO_4 and Cu_nBeF_4 analogues is the position of the two peaks mentioned above: the one of the proton in the 4-position of pz is ∼2.8 ppm less shifted than in the corresponding SO_4^{2-} and BeF_4^{2-} analogues (40.27 and 40.25 ppm, respectively), and the one of the OH proton is ∼3.7 or ∼6.2 ppm less shifted than in the SO_4^{2-} and BeF_4^{2-} analogues (−57.75 and −60.27 ppm, respectively). Because the H-bonding parameters between the nanojar and the incarcerated anion in $Cu_{28}CrO_4$ and the SO_4^{2-} and BeF_4^{2-} analogues are rather similar, the difference observed in the ^{1}H NMR spectrum is attributed to the different basicity of the anions. Indeed, CrO_4^{2-} is significantly more basic than SO_4^{2-} and BeF_4^{2-} as H_2CrO_4 is a much weaker acid (pK_1 = 0.74; pK_2 = 6.49)[60] than H_2SO_4 ($pK_1 \simeq -3$; pK_2 = 1.92)[60] and H_2BeF_4. For the latter, pK_a values are not available, but it is expected to be more acidic than H_2SO_4 due to the smaller atomic charge on F in BeF_4^{2-} (−0.95)[61] than on O in SO_4^{2-} (−1.1).[62,63] In comparison, the other nanojar rings show less variation in chemical shifts with the three different anions, the large Cu_{12} and Cu_{14} rings being the least affected ones (Table S20).

The variable-temperature (VT) ^{1}H NMR measurements in DMSO-d_6 over the 25−150 °C range show that the degree of temperature dependence of the chemical shifts of the different protons in CrO_4-nanojars is similar to the SO_4 and BeF_4 analogues (Table S20), as is the thermal stability of nanojars of different sizes (Figure 9 and Figure S18). Thus, a gradual transformation of $Cu_{6+12+10}$ and the other nanojars found in minor amounts into Cu_{8+14+9} is observed at increasing temperatures. At 150 °C, only the Cu_{8+14+9} nanojar prevails. Visual inspection of the NMR tube after the VT experiment shows no change in the appearance of the solution and the absence of any solid deposit, confirming not only the stability of the $Cu_{31}CrO_4$ nanojar at 150 °C in DMSO-d_6 but also the clean transformation of nanojars of other sizes into $Cu_{31}CrO_4$. It is worth noting the almost complete absence of the smallest $Cu_{27}CrO_4$ nanojar even at room temperature, in contrast with the $Cu_{27}SO_4$ and $Cu_{27}BeF_4$ analogues.[52,53] Again, this is attributable to the slightly larger size of the CrO_4^{2-} ion compared to SO_4^{2-} and BeF_4^{2-}.

As shown in the synthesis section above, refluxing a Cu_nCrO_4 nanojar mixture in methanol leads to virtually pure $Cu_{31}CrO_4$. The ^{1}H NMR peaks of this nanojar (especially the ones of the Cu_9 ring) suffer from severe paramagnetic relaxation enhancement and residual dipolar couplings leading to a drastic peak broadening. Thus, the peaks of the $Cu_{31}CrO_4$ nanojar are barely or not discernable in the room-temperature ^{1}H NMR spectrum of the Cu_nCrO_4 mixture (Figure 9 and Figure S18). The pure $Cu_{31}CrO_4$ sample provides a means of confirming the chemical shifts of this nanojar at ambient temperature. Figure 10 further illustrates the assignment of the pz protons in the 4- and 3/5-positions, which are present in a 1:2 ratio. Traces of other nanojar sizes seen in Figure 10 are attributable to scrambling due to the strong donor capacity of DMSO-d_6 (donor number, DN = 30)[64] compared to CH_3CN (DN = 14) used for the mass spectrometric studies, an observation that has been documented with other nanojars.[65]

UV−vis Spectroscopy. The UV−vis spectrum of Cu_nCrO_4 (n = 27−33) in THF (Figure 11) displays two peaks with absorption maxima at 351 and 602 nm, corresponding to charge-transfer and d−d transitions, respectively (with extinction coefficients of ε_{351nm} = 2.8 × 10^4 L mol^{-1} cm^{-1} and ε_{602nm} = 2.1 × 10^3 L mol^{-1} cm^{-1}). The λ_{max} values are essentially identical to the ones measured for Cu_nSO_4 (n = 27−33)[49] and Cu_nCO_3 (n = 27, 29−31).[65] The charge transfer band at λ_{max} = 373 nm (in H_2O)[38,66] responsible for the yellow color of the CrO_4^{2-} ion is obscured

https://doi.org/10.1021/acs.inorgchem.3c00262
Inorg. Chem. 2023, 62, 5716−5728

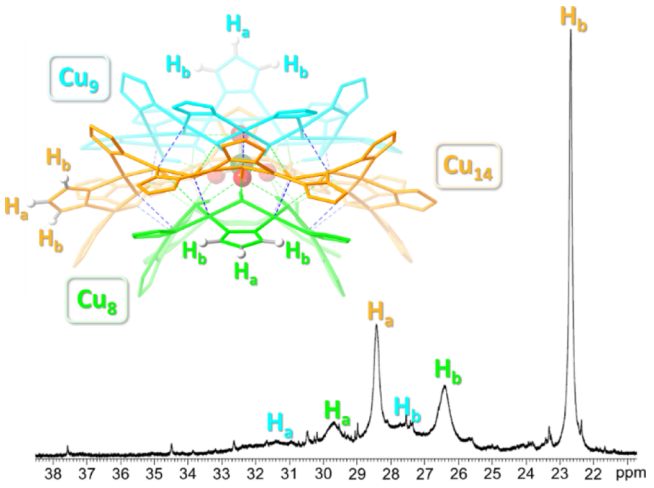

Figure 10. ^{1}H NMR spectrum of $Cu_{31}CrO_4$ in DMSO-d_6, showing pyrazolate proton signals at 25 °C.

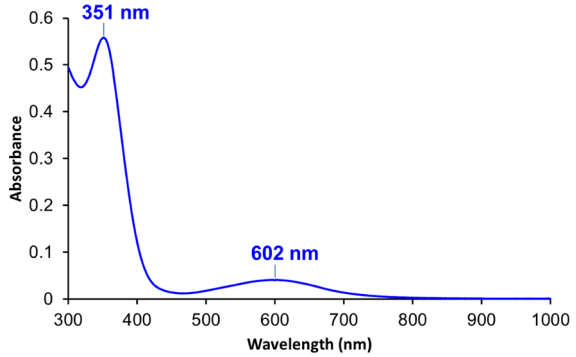

Figure 11. UV−vis spectrum of Cu_nCrO_4 (n = 27−33) in THF (20 μM).

by the strong charge-transfer band of the nanojar at λ_{max} = 351 nm.

Assessment of Chromate Binding Strength by Competitive Anion Binding. As with other nanojars studied earlier, an association constant determination by host−guest titration is precluded by the fact that a guest-free nanojar host cannot be isolated. Therefore, the binding strength of CrO_4^{2-} by nanojars was assessed by competitive binding experiments using Ba^{2+}, which could form highly insoluble $BaCrO_4$ (K_{sp} = 1.3 × 10^{-10} in H_2O).[67] Experiments were carried out both under heterogeneous conditions, by vigorously stirring a solution of Cu_nCrO_4 (n = 27−33) in water-immiscible 2-methyltetrahydrofuran (2-MeTHF) with an aqueous solution of $Ba(NO_3)_2$ followed by separation of the two layers and under homogeneous conditions by using barium dioctyl sulfosuccinate, $Ba(DOSS)_2$, which is soluble in 2-MeTHF together with the nanojar mixture. In both cases, no $BaCrO_4$ precipitate formation is observed and ESI-MS(−) of the organic layer shows no nanojar degradation products but mostly $Cu_{31}CrO_4$ and small amounts of $Cu_{28}CrO_4$ and $Cu_{32}CrO_4$ (Figure S4). For comparison, a control experiment carried out under identical conditions but by using the equivalent amount of Na_2CrO_4 instead of Cu_nCrO_4 leads to the immediate formation of a yellow $BaCrO_4$ precipitate. The amounts of $Cu_{29}CrO_4$, $Cu_{30}CrO_4$ and $Cu_{33}CrO_4$, which are present in very small amounts in the original mixture, are further reduced after stirring with Ba^{2+}, indicating a lesser preference of CrO_4^{2-} for those nanojar sizes. The results of the competitive anion binding studies imply an extremely strong binding of the CrO_4^{2-} ion by nanojars, especially by $Cu_{31}CrO_4$, which allows for the efficient removal of trace amounts of CrO_4^{2-} from water (described below).

Liquid−Liquid Extraction of CrO_4^{2-} from Water into Aliphatic Hydrocarbon Solvents. In aqueous solutions, chromate (CrO_4^{2-}), hydrogenchromate ($HCrO_4^-$) and dichromate ($Cr_2O_7^{2-}$) are in a pH and concentration-dependent equilibrium.[38] At neutral pH, chromate exists mostly as CrO_4^{2-}, which is a highly hydrophilic anion (ΔG_h° = −950 kJ/mol) similar to SO_4^{2-} (ΔG_h° = −1080 kJ/mol).[39] In alkaline solutions, CrO_4^{2-} is the only species present. Therefore, the extraction of chromate from water into aliphatic solvents at neutral or alkaline pH is difficult. Nanojars are excellent extraction agents that resist highly alkaline environments and are able to extract even the most hydrophilic anions, such as CO_3^{2-} (ΔG_h° = −1315 kJ/mol), from water at pH > 14 into aliphatic solvents.[58]

Because the parent nanojars (Cu_nCrO_4) are not soluble in aliphatic solvents, the 4-octylpyrazole derivative (4-OctpzH), which is very soluble in n-heptane, was employed instead. Extraction of chromate from an aqueous solution of Na_2CrO_4 was carried out by stirring with nanojar-forming ingredients ($Cu(NO_3)_2$, 4-OctpzH, and a base in 1:1:2 molar ratio) and n-heptane. Initially, NaOH/Bu_4NOH was used as base, resulting in water-soluble $NaNO_3$/Bu_4NNO_3 as byproducts. To prevent nitrate from accumulating in the aqueous phase, tri-n-octylamine (Oct_3N; vapor pressure < 0.001 kPa; b.p. 365 °C; flash point 168 °C; solubility in H_2O at 20 °C: 0.050 mg/L) was employed in subsequent trials. The resulting $Oct_3NH^+NO_3^-$ is soluble in the n-heptane layer but not in the aqueous phase. Further improvement was implemented by using the pre-synthesized trinuclear copper pyrazolate complex [$Cu_3(\mu_3$-OH)(μ-4-Octpz)$_3(NO_3)_2(H_2O)$] as a nanojar precursor instead of $Cu(NO_3)_2$ and 4-OctpzH. We have shown previously that the trinuclear complex can be transformed cleanly into the nanojar by reaction with a base.[56] Thus, only 20 equiv of base (Oct_3N) are needed per nanojar instead of 60 equiv, and only 18 equiv of $Oct_3NH^+NO_3^-$ are generated instead of 58 equiv when the trinuclear complex is used instead of $Cu(NO_3)_2$. An even less harmful and more environmentally friendly industrial solvent used in liquid−liquid extractions is Isopar-L, which is a colorless and odorless mixture of C_{11} − C_{13} isoalkanes, with lower vapor pressure (0.04 kPa at 20 °C, bp ∼189−209 °C) and higher flash point (61 °C) than n-heptane (vapor pressure 5.3 kPa at 20 °C, bp 98 °C, flash point −4 °C). Nanojars derived from 4-OctpzH are also very soluble in Isopar-L, which is a good alternative solvent for liquid−liquid extractions that employ nanojars as extraction agents.

The concentration of the residual chromate in the aqueous phase after extraction was determined by spectrophotometry using 1,5-diphenylcarbazide, which forms an intense red-violet complex in the presence of chromate with an absorption maximum at 540 nm.[66,68−71] The corresponding concentrations after extraction using $Cu(NO_3)_2$/4-OctpzH and [$Cu_3(\mu_3$-OH)(μ-4-Octpz)$_3(NO_3)_2(H_2O)$] were 97(±5) and 68(±5) ppb, respectively. Because quaternary ammonium salts (including trioctylammonium, which forms during the nanojar-forming reaction as a side-product) are also known to extract chromate from aqueous to organic solutions (although under highly acidic conditions),[28−32] chromate extraction was also tested with $Oct_3NH^+NO_3^-$ alone. In this case, the residual

https://doi.org/10.1021/acs.inorgchem.3c00262
Inorg. Chem. 2023, 62, 5716−5728

chromate concentration was 247(±5) ppb, indicating that Oct_3NH^+ alone is not as good an extraction agent as nanojars.

The extracted CrO_4^{2-} can be recovered from the organic layer by stripping with an acidic solution. We have shown earlier that slight acidification leads to the breakdown of nanojars to trinuclear copper pyrazolate species resulting in the release of the incarcerated anion.[53,59] Indeed, after stirring the organic layer with a dilute HNO_3 solution, addition of $Ba(NO_3)_2$ to the aqueous stripping solution causes the precipitation of the insoluble, yellow $BaCrO_4$.

CONCLUSIONS

ESI-MS studies of the as-synthesized Cu_nCrO_4 nanojar mixture document all nanojar sizes between n = 27 and n = 33 in CH_3CN solution, with $Cu_{31}CrO_4$ being the major species followed by $Cu_{28}CrO_4$ and $Cu_{32}CrO_4$. A correlation between nanojar size and anion size is observed. On the one hand, only traces of the smallest Cu_{27} nanojar form with the larger CrO_4^{2-} ion (Cr−O: 1.63 Å), whereas the Cu_{27} nanojar is more abundant with the smaller SO_4^{2-} (S−O: 1.48 Å) and BeF_4^{2-} (Be−F: 1.55 Å) ions. On the other hand, the larger Cu_{32} nanojar is much more prominent with CrO_4^{2-}, and is only observed in trace amounts with SO_4^{2-} and BeF_4^{2-}.

VT ^{1}H NMR studies confirm that Cu_nCrO_4 nanojars are also stable in the strong donor solvent DMSO-d_6, up to at least 150 °C in the case of $Cu_{31}CrO_4$. No oxidative degradation of the nanojar extraction agent is observed in the presence of the strongly oxidizing chromate.

Single-crystal X-ray crystallographic studies not only demonstrate that chromate is bound as the dinegative CrO_4^{2-} ion inside nanojars but also offer intricate details about the supramolecular binding of the anion by multiple H-bonds (12−15 bonds with O···O distances shorter than 3.2 Å, averaging 2.917(3)−2.935(5) Å in the various structures studied). In spite of the multiple H-bond donor positions available, the CrO_4^{2-} ion appears to have a strongly preferred orientation within the cavity of nanojars. Thus, in the four different $Cu_{31}CrO_4$ structures, the CrO_4^{2-} ion is found either in one single orientation or disordered over two orientations in a 0.89/0.11 or 0.95/0.05 ratio. In the smaller $Cu_{28}CrO_4$ structure, the CrO_4^{2-} ion is disordered over three orientations in a 0.62/0.19/0.19 ratio. Furthermore, the four pseudopolymorphic structures reveal that the crystallization solvent results in insignificant variations in individual bond lengths and angles within the nanojar framework, while the relative orientation between the nanojar and counterion units in the crystal lattice can lead to more drastic changes in their 3D packing and the overall crystal symmetry.

While known extraction agents for chromate only work under highly acidic conditions and extract the ion as $HCrO_4^-$ (or $ClCrO_4^-$ in the presence of Cl^- ions), nanojars are the first extraction agents capable of extracting the dinegative CrO_4^{2-} ion from neutral or alkaline aqueous solutions. Despite the large hydration energy and strong hydrophilicity of the anion (ΔG_h° = −950 kJ/mol), nanojars bind CrO_4^{2-} very strongly and can efficiently transfer it into aliphatic hydrocarbon solvents. Liquid−liquid extractions carried out with nanojars lower chromate concentrations in aqueous solutions to as low as 68(±5) ppb.

EXPERIMENTAL SECTION

General. All commercially available chemicals were used as received (solvents are ACS or HPLC grade, and THF is inhibited with 250 ppm BHT). $Cu(NO_3)_2{\cdot}2.5H_2O$ (ACS reagent, 98%), NaOH (ACS reagent, 97%), K_2CrO_4 (ACS reagent, 99%), and CrO_3 (ReagentPlus, 99.9%) were purchased from Sigma-Aldrich, pyrazole (99%) was from Oakwood Chemical, and Bu_4NOH (HPLC grade, 1.0 M in H_2O) was from Thermo Scientific. Na_2CrO_4 (Fisher Chemical, certified, 98%) was dried in an oven at 110 °C to constant weight. Deionized water was freshly boiled and cooled to room temperature under N_2(g). Tri-*n*-octylammonium nitrate,[72] Ba(DOSS)$_2$,[53] $(Bu_4N)_2[CO_3 \subset \{Cu(OH)(pz)\}_n]$ (Cu_nCO_3; n = 27, 29−31), and $(Bu_4N)_2[SO_4 \subset \{Cu(OH)(pz)\}_n]$ (Cu_nSO_4; n = 27−33) were prepared according to published procedures.[51,52] $[Cu_3(\mu_3\text{-}OH)(\mu\text{-}4\text{-}Octpz)_3(NO_3)_2(H_2O)]$ was prepared similarly to the pz-analog,[56] except that the work-up excludes trituration of the oily product with Et_2O, in which the 4-octylpyrazole derivative is soluble. Gaseous NH_3 was generated by gently heating a 30% aqueous NH_3 solution. The synthesis and reactions of nanojars were carried out under an N_2(g) atmosphere. NMR spectra were collected on a Jeol JNM-ECZS (400 MHz) instrument, and UV−Vis measurements were carried out on a Shimadzu UV-1650PC spectrophotometer.

Synthesis of Copper(II) Chromate. A solution of K_2CrO_4 (5.408 g, 27.85 mmol) in 75 mL of water was added slowly, under stirring, to a solution of $Cu(NO_3)_2{\cdot}2.5H_2O$ (6.477 g, 27.85 mmol) in 75 mL of water. The brown-red precipitate was stirred for 15 min, and then it was filtered, washed with water, and dried in an oven to afford 3.380 g (68%) of product.

Synthesis of $(Bu_4N)_2[CrO_4 \subset \{Cu(OH)(pz)\}_n]$ (Cu_nCrO_4; n = 27−33). *Method A.* $Cu(NO_3)_2{\cdot}2.5H_2O$ (10.000 g, 42.99 mmol), pyrazole (2.927 g, 42.99 mmol), NaOH (3.380 g, 84.50 mmol), Bu_4NOH (1 M in H_2O, 3.00 g, 3.00 mmol), and Na_2CrO_4 (6.964 g, 42.99 mmol) were stirred in THF (200 mL) for 3 days in a sealed flask. The deep-blue solution was filtered and the solid was rinsed with THF. Evaporation of the solvent under vacuum afforded a dark blue powder. Yield: 7.114 g (∼98%). ESI-MS(−): m/z 2051, n = 27; m/z 2125, n = 28; m/z 2199, n = 29; m/z 2272, n = 30; m/z 2346, n = 31; m/z 2420, n = 32; m/z 2494, n = 33 (Figure 1).

Method B. Copper(II) chromate (696 mg, 3.88 mmol), pyrazole (264 mg, 3.88 mmol), NaOH (299 mg, 7.48 mmol), and Bu_4NOH (1 M in H_2O, 277 mg, 0.277 mmol) were stirred in THF (15 mL) for 5 days. An orange-brown solid was filtered off and the deep-blue solution was evaporated to yield a dark blue solid (378 mg, ∼58%), which shows an ESI-MS(−) spectrum similar to the one obtained by method *a*.

Method C. To a solution of Cu_nCO_3 (n = 27−31; 121 mg, ∼2.50×10^{-5} mol) in CH_3CN (10 mL) was added 10 mL of a 5.00×10^{-3} M solution of H_2CrO_4 (obtained by dissolving solid CrO_3 in H_2O; 5.00×10^{-5} mol). After mixing, the resulting clear blue solution was left standing in a closed flask overnight. Analysis by ESI-MS(−) of the solution shows that Cu_nCO_3 was completely converted to Cu_nCrO_4. The solution was filtered, and the solvent was evaporated. The dark blue residue was washed with water (50 mL) and then dried (99 mg). The ESI-MS(−) spectrum of the product is shown in Figure 2e.

Fractionation of Cu_nCrO_4 (n = 27−33). Cu_nCrO_4 (0.3500 g) was dissolved in toluene (2.5 mL) and a deep-blue solution was obtained. Upon standing for 48 h at room temperature, a dark-blue precipitate formed. The precipitate was filtered out, washed with a small amount of toluene, and dried in a high vacuum to give a dark-blue powder (0.0899 g). The filtrate was evaporated under reduced pressure and dried in a high vacuum to afford 0.2601 g of a dark-blue powder. The ESI-MS(−) spectra of the two fractions are shown in Figure 2b,c.

Titration of Cu_nCO_3 (n = 27, 29−31) with H_2CrO_4. A 1.0×10^{-4} M solution of carbonate nanojars was prepared by dissolving Cu_nCO_3 (n = 27, 29−31) (12.1 mg, 2.5 μmol, based on an average n = 29) in acetonitrile and diluting to volume in a 25 mL volumetric flask. A 5.0×10^{-2} M solution of H_2CrO_4 was prepared by dissolving CrO_3 (255.1 mg, 2.5 mmol) in water and diluting to volume in a 50 mL volumetric flask. A 5.0×10^{-3} M H_2CrO_4 solution was prepared by diluting 2.5 mL of the aqueous H_2CrO_4 stock solution to volume in a 25 mL volumetric flask with acetonitrile.

https://doi.org/10.1021/acs.inorgchem.3c00262
Inorg. Chem. 2023, 62, 5716−5728

1 mL of the Cu_nCO_3 solution was transferred to a dram vial using a 1000 μL micropipette. 20 μL of the 5.0×10^{-3} M H_2CrO_4 solution is required per 1 mL of the 1.0×10^{-4} M nanojar solution for each molar equiv. of H_2CrO_4. A series of solutions containing 0.0, 0.5, 1.0, 1.5, 2.0, 2.5, 3.0, 3.5, 4.0, 4.5, 5.0, 6.0, 7.0, 8.0, 9.0, 10, 15, 20, 25, 30, 60, and 100 molar equivalents of H_2CrO_4 were prepared. After the addition of the H_2CrO_4, the vials were capped, swirled, and allowed to stand overnight (~14 h) in ambient conditions. The following day, the solutions were filtered before analysis by ESI-MS. Precipitate formation was observed for samples containing 3−60 equiv of H_2CrO_4. Samples containing 0−2.5 and 100 equiv of H_2CrO_4 were clear.

Reaction of Cu_nCrO_4 with NH_3. Cu_nCrO_4 (1.001 g) was dissolved in THF (25 mL) and gaseous NH_3 was bubbled through the resulting solution for 20 min. Then, the flask was stoppered, sealed with Parafilm, and left standing for 7 days. The solution was filtered, and the solvent was evaporated to give a dark blue residue (0.887 g). ESI-MS(−) shows that the product is mostly $Cu_{31}CrO_4$ (Figure 2d).

Reaction of Cu_nCrO_4 with Methanol. Cu_nCrO_4 (0.0050 g) was dissolved in methanol (3 mL), and a clear blue solution was obtained. Blue crystals started forming within an hour. After standing overnight (~14 h), blue crystals formed and the solution became lighter in color. The blue crystals and the light blue solution were separated by filtration and were characterized by ESI-MS (Figure S3).

Reflux of Cu_nCrO_4 in Methanol. Cu_nCrO_4 (0.0510 g) was dissolved in methanol (30 mL) in a 50 mL round-bottom flask, and the blue solution was refluxed for 10 h. A brown precipitate started forming within 30 min of refluxing. After cooling to room temperature, the brown precipitate was separated from the blue solution by filtration and the filtrate was characterized by ESI-MS. Then, methanol was removed under reduced pressure leaving behind a blue residue that was characterized by ESI-MS (Figure 4) and ^{1}H NMR (Figure 10).

Competitive Anion Binding under Heterogeneous Conditions. Cu_nCrO_4 (n = 27−33, 0.0976 g, ~0.02 mmol) was dissolved in 2-MeTHF (20 mL) to give a clear, blue solution, which was then cannulated over a solution of $Ba(NO_3)_2$ (0.0104 g, 0.04 mmol) in water (20 mL). After stirring vigorously for 1 h, the clear aqueous and organic layers were separated and the 2-MeTHF layer was analyzed by ESI-MS (Figure S4). A control experiment was run under identical conditions using Na_2CrO_4 (0.0032 g, 0.02 mmol) instead of Cu_nCrO_4. Upon mixing Na_2CrO_4 with aqueous $Ba(NO_3)_2$, the solution immediately turned cloudy and over time a yellow precipitate settled out at the bottom of the reaction vessel.

Competitive Anion Binding under Homogeneous Conditions. Cu_nCrO_4 (n = 27−33, 0.0972 g, 0.02 mmol) and $Ba(DOSS)_2$ (0.0198 g, 0.02 mmol) were dissolved in 2-MeTHF (20 mL) to give a clear, blue solution. The solution was stirred for 1 h and then it was analyzed by ESI-MS (Figure S4).

Liquid−Liquid Extraction of CrO_4^{2-} from Water into *n*-Heptane. *Method A.* $Cu(NO_3)_2{\cdot}2.5H_2O$ (1.3888 g, 5.971 mmol), 4-octylpyrazole (1.0766 g; 5.971 mmol), and tri-*n*-octylamine (4.2315 g, 11.96 mmol) were added to *n*-heptane (50 mL) and the mixture was stirred with 50 mL of an aqueous solution of Na_2CrO_4 (0.0153 g, 0.0945 mmol, 306 ppm) in a closed vessel for 1 h. The organic layer turned dark blue-green almost immediately. The organic phase easily separated from the aqueous phase once the stirring was stopped, and it was removed using a separatory funnel. The aqueous phase was tested for chromate using the spectrophotometric method with 1,5-diphenylcarbazide, showing a residual chromate concentration of 97(±5) ppb.

Method B. The extraction was carried out as described above, using $[Cu_3(\mu_3\text{-}OH)(\mu\text{-}4\text{-}Octpz)_3(NO_3)_2(H_2O)]$ (1.8374 g, 2.033 mmol) and tri-*n*-octylamine (2.7262 g, 7.708 mmol) in *n*-heptane (90 mL) as extractant. Testing with 1,5-diphenylcarbazide showed a residual chromate concentration in the aqueous layer of 68(±5) ppb.

Method C. The extraction was carried out as described above, using $Oct_3NH^+NO_3^-$ (0.3253 g, 0.7807 mmol) in *n*-heptane (50 mL) as the extractant. Testing with 1,5-diphenylcarbazide showed a residual chromate concentration in the aqueous layer of 247(±5) ppb.

Mass Spectrometry. Mass spectrometric analysis of the nanojars was performed with a Waters Synapt G1 HDMS instrument, using electrospray ionization (ESI). 10^{-4}−10^{-5} M solutions were prepared in CH_3CN using either solids or aliquots taken from solutions. Samples were infused by a syringe pump at 5 μL/min and nitrogen was supplied as the nebulizing gas at 500 L/h. The electrospray capillary voltage was set to −2.5 or + 2.5 kV, respectively, with a desolvation temperature of 110 °C. The sampling and extraction cones were maintained at 40 and 4.0 V, respectively, at 80 °C.

X-ray Crystallography. Single-crystals of **1**−**3** were grown at room temperature by heptane (**1**) or pentane (**2a**) vapor diffusion into a chlorobenzene solution, by vapor diffusion of hexanes into a chlorobenzene/methanol solution (**2b**), by pentane vapor diffusion into a toluene/methanol solution (**2c**), by ethanol vapor diffusion into a nitrobenzene/bromobenzene solution (**2d**), and by methanol vapor diffusion into a nitrobenzene/methanol solution (**3**) of Cu_nCrO_4 (n = 27−32). Once removed from the mother liquor, the crystals are extremely sensitive to solvent loss in ambient conditions and were quickly mounted under a cryostream (150 K) to prevent decomposition. X-ray diffraction data were collected from a single-crystal mounted atop a MiTeGen micromesh mount under Fomblin oil with a Bruker AXS D8 Quest diffractometer with a Photon III C14 charge-integrating and photon counting pixel array detector (CPAD) using a microfocus X-ray tube with multilayer optics for monochromatization with Cu-K_α (λ = 1.54178 Å) radiation. The data were collected using APEX4,[73] integrated using SAINT,[74] and scaled and corrected for absorption and other effects using SADABS.[75] The structures were solved by employing direct methods using ShelXS[76] or ShelXT[77] and refined by full-matrix least squares on F^2 using ShelXL.[78] C−H hydrogen atoms were placed in idealized positions and refined using the riding model. Further refinement details and thermal ellipsoid plots (Figures S5−S10) are provided in the SI.

■ ASSOCIATED CONTENT

Supporting Information

The Supporting Information is available free of charge at https://pubs.acs.org/doi/10.1021/acs.inorgchem.3c00262.

Additional data for mass spectrometry, X-ray crystallography and ^{1}H-NMR spectroscopy (PDF)

Accession Codes

CCDC 2235859−2235864 contain the supplementary crystallographic data for this paper. These data can be obtained free of charge via www.ccdc.cam.ac.uk/data_request/cif, or by emailing data_request@ccdc.cam.ac.uk, or by contacting The Cambridge Crystallographic Data Centre, 12 Union Road, Cambridge CB2 1EZ, UK; fax: +44 1223 336033.

■ AUTHOR INFORMATION

Corresponding Author

Gellert Mezei − *Department of Chemistry, Western Michigan University, Kalamazoo, Michigan 49008, United States;* orcid.org/0000-0002-3120-3084; Email: gellert.mezei@wmich.edu

Authors

Wisam A. Al Isawi − *Department of Chemistry, Western Michigan University, Kalamazoo, Michigan 49008, United States;* orcid.org/0000-0002-2900-1678

Christian K. Hartman − *Department of Chemistry, Western Michigan University, Kalamazoo, Michigan 49008, United States*

Pooja Singh − *Department of Chemistry, Western Michigan University, Kalamazoo, Michigan 49008, United States*

https://doi.org/10.1021/acs.inorgchem.3c00262
Inorg. Chem. 2023, 62, 5716−5728

Matthias Zeller − *Department of Chemistry, Purdue University, West Lafayette, Indiana 47907, United States;* orcid.org/0000-0002-3305-852X

Complete contact information is available at: https://pubs.acs.org/10.1021/acs.inorgchem.3c00262

Notes

The authors declare no competing financial interest.

■ ACKNOWLEDGMENTS

This material is based on work supported by the National Science Foundation under Grant No. CHE-1808554.

■ REFERENCES

(1) Costa, M.; Klein, C. B. Toxicity and Carcinogenicity of Chromium Compounds in Humans. *Crit. Rev. Toxicol.* **2006**, *36*, 155−163.
(2) Zhitkovich, A. Importance of Chromium−DNA Adducts in Mutagenicity and Toxicity of Chromium(VI). *Chem. Res. Toxicol.* **2005**, *18*, 3−11.
(3) *CRC Handbook of Chemistry and Physics*, CRC Press, 102nd ed., 2021.
(4) Anthony, J. W.; Bideaux, R. A.; Bladh, K. W.; Nichols, M. C. Eds., *Handbook of Mineralogy, Mineralogical Society of America, Chantilly, VA, USA*. http://www.handbookofmineralogy.org (accessed: January 23, 2023).
(5) Eary, L. E.; Rai, D. Kinetics of Chromium(III) Oxidation to Chromium(VI) by Reaction with Manganese Dioxide. *Environ. Sci. Technol.* **1987**, *21*, 1187−1193.
(6) Apte, D. A.; Tare, V.; Bose, P. Extent of Oxidation of Cr(III) to Cr(VI) under Various Conditions Pertaining to Natural Environment. *J. Hazard. Mater.* **2006**, *B128*, 164−174.
(7) Oze, C.; Bird, D. K.; Fendorf, S. Genesis of Hexavalent Chromium from Natural Sources in Soil and Groundwater. *PNAS* **2007**, *104*, 6544−6549.
(8) Bourotte, C.; Bertolo, R.; Almodovar, M.; Hirata, R. Natural Occurrence of Hexavalent Chromium in a Sedimentary Aquifer in Urânia, State of São Paulo Brazil. *An. Acad. Bras. Cienc.* **2009**, *81*, 227−242.
(9) Tziritis, E.; Kelepertzis, E.; Korres, G.; Perivolaris, D.; Repani, S. Hexavalent Chromium Contamination in Groundwaters of Thiva Basin Central Greece. *Bull. Environ. Contam. Toxicol.* **2012**, *89*, 1073−1077.
(10) IARC Monographs on the Evaluation of Carcinogenic Risk of Chemicals to Man. Volume 2: *Some Inorganic and Organometallic Compounds. International Agency for Research on Cancer*, Lyon, 1973.
(11) Barceloux, D. G.; Barceloux, D. Chromium. *J. Toxicol. Clin. Toxicol.* **1999**, *37*, 173−194.
(12) Moffat, I.; Martinova, N.; Seidel, C.; Thompson, C. M. Hexavalent Chromium in Drinking Water. *J. Am. Water Works Assoc.* **2018**, *110*, E22−E35.
(13) Kingston, H. M.; Cain, R.; Huo, D.; Rahman, G. M. M. Determination and Evaluation of Hexavalent Chromium in Power Plant Coal Combustion By-Products and Cost-Effective Environmental Remediation Solutions using Acid Mine Drainage. *J. Environ. Monit.* **2005**, *7*, 899−905.
(14) Ludvik, J. *Chrome Management in the Tanyard*. V.00−56379 ed., United Nations Industrial Development Organization, 2000, pp. 1−10.
(15) Gharbi, O.; Thomas, S.; Smith, C.; Birbilis, N. Chromate Replacement: What does the Future Hold? *NPJ Mater. Degrad.* **2018**, *2*, 12.
(16) *Chromium in Drinking Water*, https://www.epa.gov/sdwa/chromium-drinking-water (accessed: January 23, 2023).
(17) Eary, L. E.; Rai, D. Chromate Removal from Aqueous Wastes by Reduction with Ferrous Ion. *Environ. Sci. Technol.* **1988**, *22*, 972−977.
(18) Korak, J.; Kennedy, A.; Arias-Paic, M. *Hexavalent Chromium Treatment Technologies*. U.S. Department of the Interior, Bureau of Reclamation, Research and Development Office, Science and Technology Program, Final Report ST-2018-9085-01. https://www.usbr.gov/research/projects/download_product.cfm?id=2746 (accessed: January 23, 2023).
(19) Korngold, E.; Belayev, N.; Aronov, L. Removal of Chromates from Drinking Water by Anion Exchangers. *Sep. Purif. Technol.* **2003**, *33*, 179−187.
(20) Kumar, P. A.; Ray, M.; Chakraborty, S. Hexavalent Chromium Removal from Wastewater Using Aniline Formaldehyde Condensate Coated Silica Gel. *J. Hazard. Mater.* **2007**, *143*, 24−32.
(21) Sayin, S.; Ozcan, F.; Yilmaz, M. Synthesis and Evaluation of Chromate and Arsenate Anions Extraction Ability of a *N*-Methylglucamine Derivative of Calix[4]arene Immobilized onto Magnetic Nanoparticles. *J. Hazard. Mater.* **2010**, *178*, 312−319.
(22) Sayin, S.; Yilmaz, M. Synthesis of a New Calixarene Derivative and Its Immobilization Onto Magnetic Nanoparticle Surfaces for Excellent Extractants Toward Cr(VI), As(V), and U(VI). *J. Chem. Eng. Data* **2011**, *56*, 2020−2029.
(23) Fu, H.-R.; Wang, N.; Qin, J.-H.; Han, M.-L.; Ma, L.-F.; Wang, F. Spatial Confinement of a Cationic MOF: A SC−SC Approach for High Capacity Cr(VI)-Oxyanion Capture in Aqueous Solution. *Chem. Commun.* **2018**, *54*, 11645−11648.
(24) Agarwal, R. A. Selective and Reversible Capture of Volatile I_2 Modifying As-Synthesized 2D Cd-MOF to 3D. *Cryst. Growth Des.* **2021**, *21*, 2046−2055.
(25) Li, P.; Damron, J. T.; Veith, G. M.; Bryantsev, V. S.; Mahurin, S. M.; Popovs, I.; Jansone-Popova, S. Bifunctional Ionic Covalent Organic Networks for Enhanced Simultaneous Removal of Chromium(VI) and Arsenic(V) Oxoanions via Synergetic Ion Exchange and Redox Process. *Small* **2021**, *17*, No. 2104703.
(26) Jansone-Popova, S.; Moinel, A.; Schott, J. A.; Mahurin, S. M.; Popovs, I.; Veith, G. M.; Moyer, B. A. Guanidinium-Based Ionic Covalent Organic Framework for Rapid and Selective Removal of Toxic Cr(VI) Oxoanions from Water. *Environ. Sci. Technol.* **2019**, *53*, 878−883.
(27) Chen, X.; Dai, X.; Xie, R.; Li, J.; Khayambashi, A.; Xu, L.; Yang, C.; Shen, N.; Wang, Y.; He, L.; Zhang, Y.; Xiao, C.; Chai, Z.; Wang, S. Chromate Separation by Selective Crystallization. *Chin. Chem. Lett.* **2020**, *31*, 1974−1977.
(28) Maeck, W. J.; Kussy, M. E.; Rein, J. E. Solvent Extraction Method for the Radiochemical Determination of Chromium. *Anal. Chem.* **1962**, *34*, 1602−1604.
(29) Adam, J.; Přibil, R. Extraction with Long-Chain Amines−II. Extraction and Colorimetric Determination of Chromate. *Talanta* **1971**, *18*, 91−95.
(30) Ohashi, K.; Shikina, K.; Nagatsu, H.; Ito, I.; Yamamoto, K. Solvent Extraction of the Ion-Pairs of Chromium(VI) and Molybdenum(VI) with Trioctylmethylammonium Chloride and Benzyldimethylcetylammonium Chloride. *Talanta* **1984**, *31*, 1031−1035.
(31) Huang, Y.-H.; Chen, C.-Y.; Kuo, J.-F. Chromium(VI) Complexation with Triisooctylamine in Organic Solvents. *Bull. Chem. Soc. Jpn* **1991**, *64*, 3059−3062.
(32) Galan, B.; Urtiaga, A. M.; Alonso, A. I.; Irabien, J. A.; Ortiz, M. I. Extraction of Anions with Aliquat 336: Chemical Equilibrium Modeling. *Ind. Eng. Chem. Res.* **1994**, *33*, 1765−1770.
(33) Mann, C. K.; White, J. C. Extraction of Chromium with Trioctylphosphine Oxide from Acidic Solutions of Alkali Metal Salts. *Anal. Chem.* **1958**, *30*, 989−992.
(34) Zhang, W.; Liu, J.; Ren, Z.; Du, C.; Ma, J. Solvent Extraction of Chromium(VI) with Tri-*n*-butyl Phosphate from Aqueous Acidic Solutions. *J. Chem. Eng. Data* **2007**, *52*, 2220−2223.
(35) Aeungmaitrepirom, W.; Hagege, A.; Asfari, Z.; Vicens, J.; Leroy, M. Solvent Extraction of Selenate and Chromate Using a Diaminocalix[4]arene. *J. Inclusion Phenom. Macrocyclic Chem.* **2001**, *40*, 225−229.

(36) Bayrakci, M.; Ertul, Ş.; Yilmaz, M. Synthesis of Di-substituted Calix[4]arene-Based Receptors for Extraction of Chromate and Arsenate Anions. *Tetrahedron* **2009**, *65*, 7963−7968.
(37) Ertul, Ş.; Bayrakcı, M.; Yilmaz, M. Removal of Chromate and Phosphate Anion from Aqueous Solutions Using Calix[4]aren Receptors Containing Proton Switchable Units. *J. Hazard. Mater.* **2010**, *181*, 1059−1065.
(38) Szabó, M.; Kalmár, J.; Ditrói, T.; Bellér, G.; Lente, G.; Simic, N.; Fábián, I. Equilibria and Kinetics of Chromium(VI) Speciation in Aqueous Solution − A Comprehensive Study from pH 2 to 11. *Inorg. Chim. Acta* **2018**, *472*, 295−301.
(39) Marcus, Y. Thermodynamics of Solvation of Ions. Part 5.—Gibbs Free Energy of Hydration at 298.15 K. *J. Chem. Soc., Faraday Trans.* **1991**, *87*, 2995−2999.
(40) Maubert, B. M.; Nelson, J.; McKee, V.; Towna, R. M.; Pál, I. Selectivity for Dinegative versus Mononegative Oxoanionic Guests within a Cryptand Host. *J. Chem. Soc., Dalton Trans.* **2001**, 1395−1397.
(41) Nelson, J.; Nieuwenhuyzen, M.; Pál, I.; Town, R. M. Dinegative Tetrahedral Oxoanion Complexation; Structural and Solution Phase Observations. *Dalton Trans.* **2004**, 2303−2308.
(42) Custelcean, R.; Bonnesen, P. V.; Duncan, N. C.; Zhang, X.; Watson, L. A.; Van Berkel, G.; Parson, W. B.; Hay, B. P. Urea-Functionalized M_4L_6 Cage Receptors: Anion-Templated Self-Assembly and Selective Guest Exchange in Aqueous Solutions. *J. Am. Chem. Soc.* **2012**, *134*, 8525−8534.
(43) Rajbanshi, A.; Custelcean, R. Structure and Selectivity Trends in Crystalline Urea-Functionalized Anion-Binding Capsules. *Supramol. Chem.* **2012**, *24*, 65−71.
(44) Dutta, R.; Chakraborty, S.; Bose, P.; Ghosh, P. Aerial CO_2 Trapped as CO_3^{2-} Ions in a Dimeric Capsule That Efficiently Extracts Chromate, Sulfate, and Thiosulfate from Water by Anion-Exchange Metathesis. *Eur. J. Inorg. Chem.* **2014**, 4134−4143.
(45) Guchhait, T.; Mani, G.; Schulzke, C. Synthesis and Structural Characterization of Anion Complexes with Azacalix[2]-dipyrrolylmethane: Effect of Anion Charge on the Conformation of the Macrocycle. *Dalton Trans.* **2016**, *45*, 11781−11790.
(46) Bian, S.-D.; Wu, H.-B.; Wang, Q.-M. A Facile Template Approach to High-Nuclearity Silver(I) Alkynyl Clusters. *Angew. Chem., Int. Ed.* **2009**, *48*, 5363−5365.
(47) Liao, J.-H.; Chang, H.-W.; You, H.-C.; Fang, C.-S.; Liu, C. W. Tetrahedral-Shaped Anions as a Template in the Synthesis of High-Nuclearity Silver(I) Dithiophosphate Clusters. *Inorg. Chem.* **2011**, *50*, 2070−2072.
(48) Jacobson, B. L.; Quiocho, F. A. Sulfate-Binding Protein Dislikes Protonated Oxyacids: A Molecular Explanation. *J. Mol. Biol.* **1988**, *204*, 783−787.
(49) Fernando, I. R.; Surmann, S. A.; Urech, A. A.; Poulsen, A. M.; Mezei, G. Selective Total Encapsulation of the Sulfate Anion by Neutral Nano-Jars. *Chem. Commun.* **2012**, *48*, 6860−6862.
(50) Mezei, G.; Baran, P.; Raptis, R. G. Anion Encapsulation by Neutral Supramolecular Assemblies of Cyclic Cu^{II} Complexes: A Series of Five Polymerization Isomers, $[\{cis\text{-}Cu^{II}(\mu\text{-}OH)(\mu\text{-}pz)\}_n]$, n= 6, 8, 9, 12, and 14. *Angew. Chem., Int. Ed.* **2004**, *43*, 574−577.
(51) Ahmed, B. M.; Szymczyna, B. R.; Jianrattanasawat, S.; Surmann, S. A.; Mezei, G. Survival of the Fittest Nanojar: Stepwise Breakdown of Polydisperse Cu_{27}−Cu_{31} Nanojar Mixtures into Monodisperse $Cu_{27}(CO_3)$ and $Cu_{31}(SO_4)$ Nanojars. *Chem. − Eur. J.* **2016**, *22*, 5499−5503.
(52) Ahmed, B. M.; Hartman, C. K.; Mezei, G. Sulfate-Incarcerating Nanojars: Solution and Solid-State Studies, Sulfate Extraction from Water, and Anion Exchange with Carbonate. *Inorg. Chem.* **2016**, *55*, 10666−10679.
(53) Al Isawi, W. A.; Zeller, M.; Mezei, G. Supramolecular Incarceration and Extraction of Tetrafluoroberyllate from Water by Nanojars. *Inorg. Chem.* **2022**, *61*, 8611−8622.
(54) Clever, H. L.; Johnston, F. J. The Solubility of Some Sparingly Soluble Lead Salts: An Evaluation of the Solubility in Water and Aqueous Electrolyte Solution. *J. Phys. Chem. Ref. Data* **1980**, *9*, 751−784.
(55) (a) Baes, C. F., Jr.; Mesmer, R. E. *The Hydrolysis of Cations*, Wiley, 1976. (b) Hawkes, S. J. All Positive Ions Give Acid Solutions in Water. *J. Chem. Educ.* **1996**, *73*, 516−517.
(56) Ahmed, B. M.; Mezei, G. From Ordinary to Extraordinary: Insights into the Formation Mechanism and pH-Dependent Assembly/Disassembly of Nanojars. *Inorg. Chem.* **2016**, *55*, 7717−7728.
(57) Huybrechts, M.; Degard, C. The Solubility of Lead Chromate. Application to the Titration of Lead. *Bull. Soc. Chim. Belg.* **1933**, *42*, 331−346.
(58) Ahmed, B. M.; Calco, B.; Mezei, G. Tuning the Structure and Solubility of Nanojars by Peripheral Ligand Substitution, Leading to Unprecedented Liquid−Liquid Extraction of the Carbonate Ion from Water into Aliphatic Solvents. *Dalton Trans.* **2016**, *45*, 8327−8339.
(59) Al Isawi, W. A.; Zeller, M.; Mezei, G. Isomorphous but No Dead Ringer: Contrasting the Supramolecular Binding of Tetrafluoroberyllate and Sulfate Ions by Nanojars. *Cryst. Growth Des.* **2023**, *23*, 1676−1688.
(60) Perrin, D. D. *Ionization Constants of Inorganic Acids and Bases in Aqueous Solution*, 2nd ed., Pergamon, Oxford, 1982.
(61) Robinson, E. A.; Johnson, S. A.; Tang, T.-H.; Gillespie, R. J. Reinterpretation of the Lengths of Bonds to Fluorine in Terms of an Almost Ionic Model. *Inorg. Chem.* **1997**, *36*, 3022−3030.
(62) Cannon, W. R.; Pettitt, B. M.; McCammon, J. A. Sulfate Anion in Water: Model Structural, Thermodynamic, and Dynamic Properties. *J. Phys. Chem.* **1994**, *98*, 6225−6230.
(63) Smeeton, L. C.; Farrell, J. D.; Oakley, M. T.; Wales, D. J.; Johnston, R. L. Structures and Energy Landscapes of Hydrated Sulfate Clusters. *J. Chem. Theory Comput.* **2015**, *11*, 2377−2384.
(64) Gutmann, V. *The Donor-Acceptor Approach to Molecular Interactions*, 1st ed.; Springer: US, 1978.
(65) Al Isawi, W. A.; Zeller, M.; Mezei, G. Capped Nanojars: Synthesis, Solution and Solid-State Characterization, and Atmospheric CO_2 Sequestration by Selective Binding of Carbonate. *Inorg. Chem.* **2021**, *60*, 13479−13492.
(66) Sanchez-Hachair, A.; Hofmann, A. Hexavalent Chromium Quantification in Solution: Comparing Direct UV-visible Spectrometry with 1,5-Diphenylcarbazide Colorimetry. *C. R. Chim.* **2018**, *21*, 890−896.
(67) Beyer, G. L.; Rieman, W., III The Solubility Product of Barium Chromate at Various Ionic Strengths. *J. Am. Chem. Soc.* **1943**, *65*, 971−973.
(68) Pflaum, R. T.; Howick, L. C. The Chromium-Diphenylcarbazide Reaction. *J. Am. Chem. Soc.* **1956**, *78*, 4862−4866.
(69) Dean, J. A.; Beverly, M. L. Extraction and Colorimetric Determination of Chromium with 1,5-Diphenylcarbohydrazide. *Anal. Chem.* **1958**, *30*, 977−979.
(70) Noroozifar, M.; Khorasani-Motlagh, M. Specific Extraction of Chromium as Tetrabutylammonium-Chromate and Spectrophotometric Determination by Diphenylcarbazide: Speciation of Chromium in Effluent Streams. *Anal. Sci.* **2003**, *19*, 705−708.
(71) Ma, J.; Yang, B.; Byrne, R. H. Determination of Nanomolar Chromate in Drinking Water with Solid Phase Extraction and a Portable Spectrophotometer. *J. Hazard. Mater.* **2012**, *219-220*, 247−252.
(72) Katsuta, S.; Yoshimoto, Y.; Okai, M.; Takeda, Y.; Bessho, K. Selective Extraction of Palladium and Platinum from Hydrochloric Acid Solutions by Trioctylammonium-Based Mixed Ionic Liquids. *Ind. Eng. Chem. Res.* **2011**, *50*, 12735−12740.
(73) *Bruker APEX4*. Bruker AXS Inc., Madison, Wisconsin, USA, 2019.
(74) *Bruker SAINT v.8.38A. Bruker*, Madison, Wisconsin, USA, 2017.
(75) Krause, L.; Herbst-Irmer, R.; Sheldrick, G. M.; Stalke, D. Comparison of Silver and Molybdenum Microfocus X-Ray Sources for Single-Crystal Structure Determination. *J. Appl. Crystallogr.* **2015**, *48*, 3−10.

https://doi.org/10.1021/acs.inorgchem.3c00262
Inorg. Chem. 2023, 62, 5716−5728

(76) Sheldrick, G. M. A Short History of *SHELX*. *Acta Crystallogr., Sect. A: Found. Crystallogr.* **2008**, *A64*, 112−122.
(77) Sheldrick, G. M. *SHELXT* − Integrated Space-Group and Crystal-Structure Determination. *Acta Crystallogr., Sect. A: Found. Adv.* **2015**, *A71*, 3−8.
(78) Sheldrick, G. M. Crystal Structure Refinement with SHELXL. *Acta Crystallogr., Sect. C:Struct. Chem.* **2015**, *C71*, 3−8.

https://doi.org/10.1021/acs.inorgchem.3c00262
Inorg. Chem. 2023, 62, 5716−5728